Photodissociation of Peroxynitric Acid in the Near-IR

Coleen M. Roehl,* Sergey A. Nizkorodov, and Hui Zhang

Division of Geological and Planetary Sciences, California Institute of Technology, Pasadena, California 91125

Geoffrey A. Blake

Divisions of Geological and Planetary Sciences and Chemistry and Chemical Engineering, California Institute of Technology, Pasadena, California 91125

Paul O. Wennberg

Divisions of Geological and Planetary Sciences and Engineering and Applied Science, California Institute of Technology, Pasadena, California 91125

Temperature-dependent near-IR photodissociation spectra were obtained for several vibrational overtone transitions of peroxynitric acid (HNO_4) with a tunable OPO photolysis/OH laser-induced-fluorescence system. Band-integrated photodissociation cross-sections ($\int \sigma_{diss}$), determined relative to that for the $3\nu_1$ OH stretching overtone, were measured for three dissociative bands. Assuming unit quantum efficiency for photodissociation of $3\nu_1$ we find $2\nu_1 + \nu_3$ (8242 cm^{-1}) = (1.21×10^{-20}) (independent of temperature), $2\nu_1$ (6900 cm^{-1}) = $4.09 \times 10^{-18} * e^{(-826.5/T)}$ (295 K > T > 224 K), and $\nu_1 + 2\nu_3$ (6252 cm^{-1}) = $1.87 \times 10^{-19} * e^{(-1410.7/T)}$ (278 K > T > 240 K) cm^2 molecule^{-1} cm^{-1}. The photodissociation cross-sections are independent of pressure over the range 2 to 40 Torr. Temperature-dependent quantum yields (ϕ) for these transitions were obtained using integrated absorption cross-sections ($\int \sigma_{abs}$) of HNO_4 overtone vibrations measured with a FTIR spectrometer. In the atmosphere, photodissociation in the infrared is dominated by excitation of the first overtone of the OH stretching vibration ($2\nu_1$). Inclusion of all dissociative HNO_4 overtone and combination transitions yields a daytime IR photolysis rate of approximately 1×10^{-5} s^{-1}. This process significantly shortens the estimated lifetime of HNO_4 in the upper troposphere and lower stratosphere.

I. Introduction

Chemistry in Earth's atmosphere is typically initiated by photolysis of photolabile compounds via excitation to dissociative electronic states, usually in the ultraviolet. Donaldson et al.[1] have suggested, however, that photodissociation by excitation of vibrational overtone transitions may be important for a number of atmospherically relevant compounds. In particular, they calculated that excitation of overtones of the OH stretching vibrations could significantly reduce the atmospheric lifetimes of hydrogen peroxide, nitric acid, and peroxynitric acid (HNO_4). The idea here is that the significantly higher actinic flux in the visible/near-infrared can more than compensate for the very weak band strengths of these transitions. Because the OH overtone band intensities decrease by approximately 1 order of magnitude for each additional quantam of excitation,[2−4] this process most strongly influences the chemistry of HNO_4 as it contains the weakest bond ($D_0(HO_2-NO_2) = 95.3 \pm 3.4$ kJ/mol.[5]) It was suggested by Donaldson et al.[1] that excitation of the 2nd and 3rd overtone of the OH stretch in HNO_4 would be fully dissociative. In this work, we have investigated the photodissociation cross sections for HNO_4 between 900 and 2000 nm.

HNO_4 has been observed in the atmosphere[6] and is calculated to play a significant role in the chemistry of the nitrogen and hydrogen free radical families.[7] It is thought to be formed exclusively in the gas phase via the reaction

$$HO_2 + NO_2 + M \rightarrow HNO_4 + M \qquad (1)$$

Thermal decomposition (reaction −1) is fast in the lower atmosphere. Above 7 km, however, the lifetime with respect to this process becomes long (>1 day) compared with the other known loss processes:

$$HNO_4 + h\nu \rightarrow HO_2 + NO_2 \qquad (2a)$$
$$\rightarrow OH + NO_3 \qquad (2b)$$

and

$$OH + HNO_4 \rightarrow \text{products} \qquad (3)$$
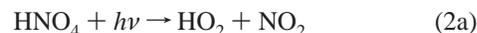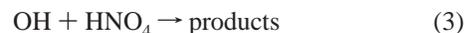
Assuming the products of reaction 3 are H_2O, O_2, and NO_2, the combination of reactions 1 and 3 represents a NO_x-catalyzed loss of odd hydrogen radicals ($HO_x = OH + HO_2$):

$$OH + HO_2 \rightarrow H_2O + O_2 \qquad (1 + 3)$$
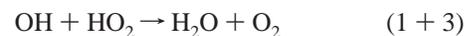
Calculations suggest that in the stratosphere[7] and at higher NO_x concentrations in the upper troposphere[8,9] this process represents a significant sink of odd-hydrogen radicals. Photolysis (reaction 2) on the other hand is a null cycle with respect to HO_x loss.

* Author to whom correspondence should be addressed. Fax: 626-585-1917. E-mail: coleen@gps.caltech.edu.

Photodissociation of Peroxynitric Acid

J. Phys. Chem. A, Vol. 106, No. 15, 2002 **3767**

An underestimate of the photolysis rate therefore leads to an underestimate of the concentration of OH.

Evidence for significant photodissociation of HNO_4 in the red or near-infrared region of the spectrum was presented by Wennberg et al.[10] Measurements of the concentration of OH and HO_2 obtained in the lower stratosphere with the sun at the horizon (that is when the atmosphere is screened from light, λ < 700 nm, by absorption and scattering) suggested a large, but unknown, near-IR source of these free radicals. Wennberg et al. were able to significantly improve the simulations of the HO_x measurements assuming that absorption, arbitrarily placed at 800 nm, produced a photolysis rate of 1×10^{-5} s^{-1} for HNO_4.[10] This rate exceeds by nearly an order of magnitude, however, the photolysis rate of HNO_4 calculated from the absorption in the 2nd and 3rd OH overtones even if a 100% dissociation efficiency is assumed for these transitions.[11]

In this work, we have combined near-IR tunable laser photodissociation spectroscopy with absorption cross-section measurements to estimate the absolute photodissociation quantum yield for a number of vibrational bands of HNO_4. We have discovered that photoexcitation of the first OH stretching overtone (near 6900 cm^{-1}) provides the dominant contribution to the near-infrared photolysis of HNO_4. The energy supplied by this excitation is, however, significantly less than the 0 K dissociation threshold (D_0); it appears that a combination of internal rotational and vibrational energy as well as collisional energy transfer to the photoexcited HNO_4, closes the energy deficit. We find that, under typical conditions of the upper troposphere/lower stratosphere, the combined effect of the infrared transitions yields a clear-sky photolysis rate for HNO_4 of approximately 1×10^{-5} s^{-1}. In the lower stratosphere and upper troposphere, the 24-hour average photolysis rate due to overtone excitation often exceeds that due to electronic excitation in the UV.

II. Experiment

A. Synthesis of HNO_4. Preparation of HNO_4 was as described by Kenley et al.[12] Briefly, ~1 g of NO_2BF_4 (Aldrich, 95%) was slowly added to ~5 mL of 95+%, chilled H_2O_2 (distilled from 70 wt %) in a N_2-purged glovebox. Once synthesized, the HNO_4 solution was transferred to a sealed glass bubbler, which was immersed in an ice/water bath. HNO_4 was introduced into the gas phase by passing pre-cooled N_2 flow through the bubbler. An alternative preparation of aqueous HNO_4 solutions based on the method described by Appelman[13] was also used for some photodissociation studies.

B. HNO_4 Absorption Cross-Sections. The HNO_4 absorption spectrum was determined over the spectral region of 1200–10500 cm^{-1} using a commercial Fourier Transform infrared (FTIR) spectrometer, equipped with a MCT-A detector, a CaF_2 beam splitter, a white light source, and a jacketed, multipass glass sample cell with CaF_2 windows. Measurements were conducted with a flowing source of HNO_4; a carrier flow of N_2 was introduced via a flow controller (at 40 sccm) upstream of the bubbler. Pressure inside the absorption cell and bubbler was monitored with a 1000 Torr (full scale) capacitance pressure transducer and was maintained at ~30 Torr by adjusting a Teflon needle valve between the cell and a pump system. Chilled methanol was circulated through the jacket of the cell to maintain a temperature of 273 K. Spectra were obtained at a resolution of 8 cm^{-1}. Since H_2O_2, HNO_3, and H_2O impurities were present in every HNO_4 synthesis, reference spectra of these gases were obtained under similar conditions to allow spectral decomposition. NO_2, which is also seen in the HNO_4 spectra, does not overlap with any of the HNO_4 features.
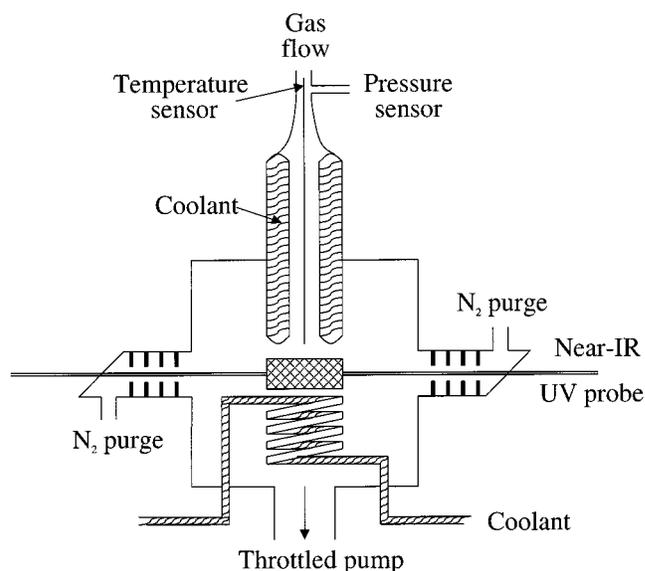
Figure 1. A schematic diagram of the OH LIF chamber (top view) used for recording photodissociation spectra. The N_2/HNO_4/NO gas mixture passes through a jacketed cooled inlet into the wall-free detection area, where it is intersected by collinear near-IR photolysis and UV probe laser beams. Resulting OH fluorescence is collected from the shaded area perpendicular both to the gas flow and to the lasers. To achieve a better temperature uniformity, the cell is additionally cooled at the gas exit area and at the optical baffles with chilled methanol running inside coiled refrigerator tubes. Cell temperature is sensed by a calibrated thermistor and pressure is measured with a capacitance manometer.

C. Photodissociation Spectra. The photodissociation spectnrum of HNO_4 was obtained using a tunable optical parametric oscillator (OPO) laser system[14] coupled with a sensitive hydroxyl radical detection system.[15] The photolysis laser is a type II BBO OPO (developed at Caltech) pumped by the 3rd harmonic (355 nm) of a pulsed Nd:YAG laser. At a Nd:YAG pulse repetition rate of 100 Hz, some 2–4 mJ/pulse of radiation is produced in the idler beam of the OPO at wavelengths between 800 and 2200 nm with a frequency width of a few wavenumbers. Radiation (idler, signal, and residual 355 nm) exiting from the OPO passes through a 700 nm long-pass filter placed at an angle to remove the 355 nm and the OPO signal and to guide a small fraction of the OPO signal into a pulsed wavemeter for accurate frequency determination. The idler beam is collimated to a size of ~4 mm^2 and directed through the photolysis chamber containing HNO_4 before being intercepted by a thermal power meter. A schematic of the laser-induced-fluorescence (LIF) chamber is shown in Figure 1. A mechanical shutter is utilized to modulate the photolysis beam, allowing for differentiation between the photolysis signal and background signal produced by the UV probe laser scatter, photolysis of HNO_4 by the UV probe laser, and HNO_4 thermal decomposition. The latter represents the major contribution to the background above 273 K and disappears almost completely below 253 K.

Co-aligned with the photolysis laser is a second laser beam used to excite OH fluorescence. Tunable ultraviolet (UV) light is produced by frequency doubling the output of a dye laser which is pumped by a frequency-doubled, diode-pumped Nd:YAG laser operated at 5–8 kHz pulse repetition frequency. This radiation (<1.0 μJ pulse^{-1}), near 282 nm, is used to pump the OH molecules into the first vibrationally excited level of the A-state. Subsequent collisions with nitrogen bath gas rapidly relax OH into the A($v = 0$) state. OH fluorescence near 309 nm is detected in a single-photon counting mode by a photo-

TABLE 1: Absolute Integrated Band Strengths of HNO$_4$ Fundamental and Overtone Vibrational Transitions (in cm^2 molecule cm^{-1}) Used in This Work[a]

band and center (cm^{-1})		$4\nu_1$ 13105	$3\nu_1$ 10090	$2\nu_1 + \nu_3$ 8240	$2\nu_1$ 6900	$\nu_1 + 2\nu_3$ 250	ν_1 3540	ν_2 1728	ν_3 1397	ν_4 1304
$\int \sigma_{abs}$	previous measurements	3.0 ± 1.8 $\times 10^{-21\ b}$	3.8 ± 1.1 $\times 10^{-20\ b}$				6.10 ± 0.73 $\times 10^{-18\ c}$	4.90 ± 0.59 $\times 10^{-17\ c}$	1.25 ± 0.18 $\times 10^{-17\ c}$	3.08 ± 0.46 $\times 10^{-1\ c}$
	this work		3.3 ± 0.7 $\times 10^{-20}$	1.6 ± 0.3 $\times 10^{-20}$	9.5 ± 1.9 $\times 10^{-19}$	2.7 ± 0.5 $\times 10^{-20}$	7.2 ± 1.4 $\times 10^{-18}$			

[a] The relative integrated band absorbances obtained from the FTIR measurements (second row) were normalized to the integrated band strength of the $3\nu_1$ overtone reported in Zhang et al.[11] and the band strength of ν_1, reported in May and Friedl.[16] [b] Ref 11. [c] Ref 16.

multiplier tube perpendicular to the gas flow and laser axes as described elsewhere.[15]

As in the absorption experiments, HNO$_4$ is introduced into the flow with N$_2$ carrier gas. The gases then pass through a jacketed, glass inlet line and eventually into a cooled flow system. The pressure in the HNO$_4$ bubbler (30−100 Torr) is monitored with a 1000 Torr (full scale) capacitance pressure transducer and is adjusted using a Teflon needle valve located between the bubbler and the photolysis chamber. Pressure in the flow (2−40 Torr) is measured with 10 and 100 Torr capacitance pressure transducers. Typical HNO$_4$ concentrations in the flow are $(5-30) \times 10^{13}$ molecule cm^{-3} estimated from the parallel FTIR measurements. The circulation of chilled methanol maintains temperature control between 300 and 223 K as measured by a calibrated thermistor.

At photolysis wavelengths greater than 950 nm, HO$_2$ is expected to be the major photoproduct of HNO$_4$ photolysis (Reaction 2a); the formation of OH is energetically precluded. Conversion of HO$_2$ to OH is achieved by addition of NO to the gas flow via

$$HO_2 + NO \rightarrow OH + NO_2 \qquad (4)$$
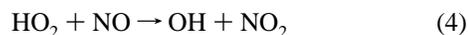
The NO density of approximately 2×10^{14} molecule cm^{-3} is chosen to ensure complete conversion to OH in less than half a millisecond, as directly verified in separate variable pump−probe delay measurements. Subsequent removal of OH occurs on a time scale of a few milliseconds consistent with reaction 3 being the primary OH loss mechanism in the flow tube. At higher NO relative densities and total pressures the three body recombination process

$$HO + NO + M \rightarrow HONO + M \qquad (5)$$

contributes to the OH loss as well. At the experimental pressures and NO concentrations employed, recombination via HO$_2$ + NO$_2$ is unimportant.

III. Results

Near- and mid-infrared HNO$_4$ absorption spectra were measured using a FTIR spectrometer. Fundamental vibrational modes ($\nu_1 - \nu_4$) of HNO$_4$ were identified in the mid-IR region between 1200 and 3700 cm^{-1} and their relative strengths were determined. The relative band intensities of the fundamentals ($\int \sigma_{abs}$) were found to be within 7% of those measured by May and Friedl.[16] Two combination bands, located at 6252 and 8242 cm^{-1}, and $2\nu_1$ and $3\nu_1$, the overtone bands, were also observed in the near-IR. Absolute integrated absorption cross-sections for these near-IR bands were calculated using the known band intensities of $3\nu_1$[11] and ν_1.[16] A comparison of the near-IR integrated absorption cross-sections is given in Table 1 and the near-IR features are shown in Figure 2 along with the ν_1 fundamental. The strengths of the stronger fundamentals (ν_2-
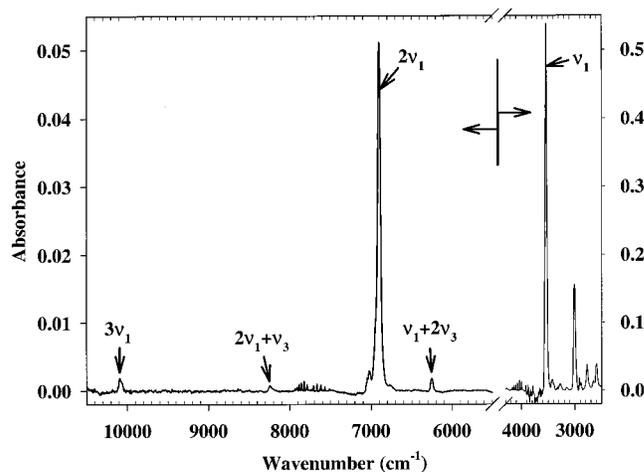
Figure 2. Absorption spectrum of HNO$_4$ between 2500 and 10500 cm^{-1}. The spectrum below 4300 cm^{-1} corresponds to the right ordinate, while the near-IR portion (above 5500 cm^{-1}) corresponds to the left ordinate.

ν_4) could not be reliably measured simultaneously with ν_1 and the overtones because of the high number density of HNO$_4$ used.

Uncertainties in the HNO$_4$ band strengths arise from several factors including baseline drifts, the signal-to-noise ratio in the FTIR spectra ($\sim$30/1 at 10000 cm^{-1}), and uncertainty in the absolute band intensities of $3\nu_1$ and ν_1. Impurities also affect the precision of the band intensity measurements because all of the HNO$_4$ bands overlap somewhat with HNO$_3$, H$_2$O$_2$, and H$_2$O bands. HNO$_3$ in particular is difficult to account for because of the strong overlap of the bands. Great care was taken to subtract the impurities from the FTIR spectra of HNO$_4$. Nevertheless, the literature values for the absolute band intensities of $3\nu_1$ and ν_1 (3.8×10^{-20} and 6.10×10^{-18} cm^2 molecule^{-1} cm^{-1}, respectively[11,16]) are not consistent within the measurements uncertainties with the relative strengths determined here and we have chosen to split the difference. A value of $3\nu_1 = 3.3 \times 10^{-20}$ cm^2 molecule^{-1} cm^{-1} was used in the normalization to obtain the band strengths reported in Table 1; the quoted errors reflect the uncertainty in $3\nu_1$. Errors in the integrated band strengths propagate directly into the integrated photodissociation cross-sections reported below.

Near-IR induced dissociation of HNO$_4$ is evidenced here by the LIF detection of OH following HNO$_4$ IR excitation and conversion of HO$_2$ to OH in reaction with NO. The OH LIF signal requires both IR and UV probe radiation and appears only in the presence of NO. Figure 3 shows a sample photodissociation spectrum obtained by scanning the excitation frequency of the near-IR laser in the region of the OH stretch overtone. Several distinct dissociative bands attributable to various HNO$_4$ overtone and combination bands are observed in the photolysis frequency range 5000 to 11000 cm^{-1}. No known impurities present in the HNO$_4$ solution (e.g., HNO$_3$) produce IR-induced OH LIF signals under such conditions

Photodissociation of Peroxynitric Acid

J. Phys. Chem. A, Vol. 106, No. 15, 2002 **3769**
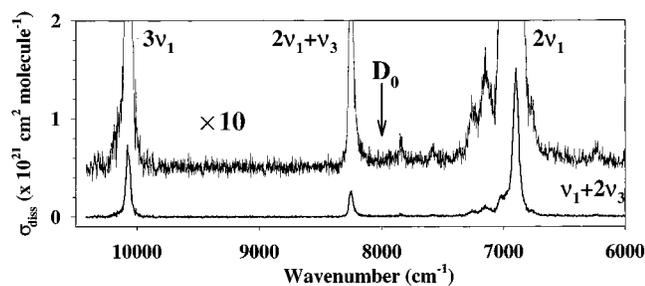
Figure 3. A sample photodissociation spectrum of HNO_4 recorded at 243 K. In addition to the OH stretching overtones $2\nu_1$ and $3\nu_1$, several weaker features are visible between 6000 and 8000 cm^{-1}. They are assigned to combinations of ν_1 and $2\nu_1$ with other HNO_4 vibrations. The position of the dissociation energy of HNO_4 is marked with an arrow. The magnified spectrum (offset for clarity) shows no evidence of dissociation between bands. The relative intensities are not accurate in this spectrum as it was taken under slightly saturated conditions.
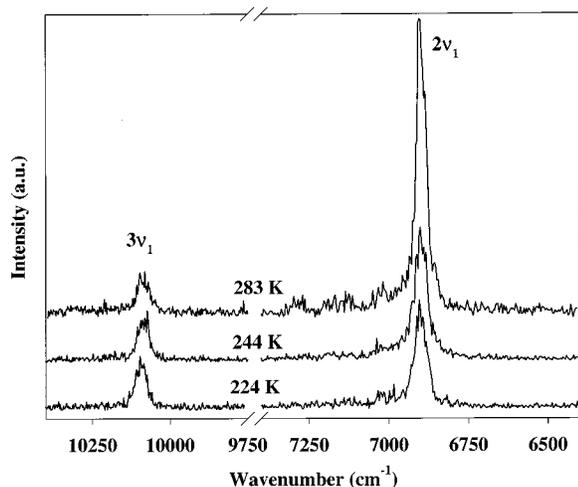
Figure 4. The effect of temperature on the photodissociation band intensities. The intensity of the $2\nu_1$ band relative to that of the $3\nu_1$ band increases markedly with temperature. The spectra are scaled to have the same area of the $3\nu_1$ band and offset for clarity.

giving strong additional evidence that it comes from HNO_4. The photodissociation signal was found to vary linearly with laser power of both the UV-LIF and IR radiation. The relative band intensities did not depend on the fraction of NO present in the cell (50–1300 ppmv) or the total gas pressure (2–40 Torr).

Photodissociation spectra of four selected bands, namely the $3\nu_1$ OH-stretch overtone, a combination band assigned to $2\nu_1 + \nu_3$, the $2\nu_1$ OH-stretch overtone, and a second combination transition tentatively assigned to $\nu_1 + 2\nu_3$, were examined as a function of temperature. All these bands are also observable in the FTIR spectrum of HNO_4 (Figure 2). After accounting for variations in the IR laser power and removing the background signal due to the UV probe laser scatter, UV photolysis of HNO_4, and HNO_4 thermal decomposition, integrated band dissociation cross-sections at each temperature were calculated relative to $3\nu_1$. To minimize the effect of small drifts in the probe laser power and/or changes in the HNO_4 concentration on the relative intensity measurements, all photodissociation scans were immediately followed and/or preceded by scans over the $3\nu_1$ reference band. While the normalized intensity of the $2\nu_1 + \nu_3$ combination band is independent of temperature, both $2\nu_1$ and $\nu_1 + 2\nu_3$ combination band exhibited strong temperature dependence. This dependence is demonstrated for $2\nu_1$ in Figure 4, which shows photodissociation spectra normalized for constant $3\nu_1$ taken at 283, 244, and 224 K.

TABLE 2: Vibrational Frequencies of HNO_4 (in cm^{-1}) Observed in Combination with the $2\nu_1$ Vibration (centered at 6900 cm^{-1}) Compared to the Known Experimental[13,17,18] and Theoretical[19] Frequencies of PNA Fundamentals[a]

band center (±10 cm^{-1})	band center $-2\nu_1$ center	tentative assignment	ab initio frequencies	experimental frequencies
7020	120	O–NO_2 torsion (ν_{12})	134	154[b]
7150	250	asym. NOO/ONO bend	298	
7260	360	HOON torsion (ν_{11})	377	340
7580	680	sym. NOO/ONO bend	682	648
7840	940	OO stretch (ν_5)	988	940
8240	1340	OOH bend (ν_3)	1452	1397

[a] The vibrational labels are from Friedl et al.[18] The correctness of the assignment of the NOO/ONO bend fundamentals is still debated. [b] Observed only in combination with the NO stretch of Friedl et al.[18]

IV. Discussion

A. Vibrational Assignment. The exceptional sensitivity offered by the method of photodissociation spectroscopy enables observation of very weak vibrational bands, some of which are either well below the detection limit of the absorption measurements or obscured by the impurities. Three reproducible features appear in the photodissociation spectrum on the blue side of the $2\nu_1$ band separated by some 120, 250, and 350 cm^{-1} from the $2\nu_1$ band center (Figure 3). Two additional extremely weak features are visible 680 and 940 cm^{-1} above $2\nu_1$. Finally, a stronger feature is observed 1350 cm^{-1} above $2\nu_1$, which is also easily discernible in the FTIR spectrum (Figure 2). The bands presumably correspond to combinations of $2\nu_1$ with various lower frequency modes of HNO_4. The tentative assignment of these bands is based on the comparison with known fundamental vibrations of HNO_4[13,17–19] as given in Table 2 and discussed further below.

The agreement between the observed vibrational frequencies of HNO_4 in the $2\nu_1$ state and the experimental frequencies of HNO_4 fundamentals (Table 2) is quite reasonable and is also consistent with the anticipated direction of frequency shifts due to the cross anharmonicities. For example, an excitation of the OH stretch is expected to lower the OOH bending frequency somewhat prompting the assignment of the 8250 cm^{-1} band to a combination of the first OH stretching overtone ($2\nu_1$) with the OOH bending vibration (ν_3). An alternative assignment of this band to a combination of $2\nu_1$ with the NO_2 symmetric stretch (ν_4), which is a very bright vibration at 1304 cm^{-1} in the fundamental range of the spectrum, would require an unphysically large coupling between the OH stretch and vibrations localized on the NO_2 end of the molecule. Similarly, excitation of $2\nu_1$ should have little influence on the OO stretch (ν_5), in agreement with our observations (Table 2). The reason for the relatively large difference in the frequency of the symmetric NOO/ONO bend (680 cm^{-1} vs 648 cm^{-1}) is not clear at present, however the correctness of this assignment is still being debated.[19]

A possible alternative assignment for the lowest frequency feature at 7020 cm^{-1} in the blue wing of $2\nu_1$ would be that of a sequence band of type $2\nu_1 + \nu_x - \nu_x$. A shift of 120 cm^{-1} between $2\nu_1$ and its sequence band would then imply a fairly large interaction between ν_1 and ν_x modes induced, perhaps, by a strong hydrogen bonding between the H atom and an oxygen atom of the NO_2 group. However, the existence of such an interaction is not consistent with the predicted non-hydrogen bonded equilibrium structure of HNO_4,[19] and also with the small observed effect on the frequency of the HOON torsion (ν_{11}) induced by the $2\nu_1$ excitation. One way to definitively disqualify the sequence band assignment is to carefully compare the

relative intensities of the $2\nu_1$ and 7020 cm^{-1} bands in the photodissociation and FTIR spectra. If the 7020 cm^{-1} band were a sequence, it would access a significantly higher energy level in the upper state compared to $2\nu_1$ and, therefore, dissociate with an increased quantum yield. Our measurements suggest that this is not the case, although a large interference from HNO$_3$ and H$_2$O$_2$ impurities makes qualitative measurements of FTIR intensities between 7000 and 7300 cm^{-1} quite difficult. In conclusion, the weak bands between $2\nu_1$ and $3\nu_1$ can all be confidently assigned to different $2\nu_1 + \nu_x$ combinations as shown in Table 2.

B. Photodissociation Quantum Yields. Two separate pieces of spectroscopic information are required to estimate the photodissociation quantum yields. The FTIR absorption spectrum of HNO$_4$ provides relative integrated band strengths for different fundamental and overtone vibrations of HNO$_4$ (Table 1). All infrared active vibrations appear in the absorption spectrum irrespective of the subsequent fate of the photoexcited peroxynitric acid molecules. In the photodissociation spectrum (Figure 3), only excitations resulting in the fragmentation of peroxynitric acid are observed. The latter can be thought of as a convolution between the absorption spectrum and photodissociation quantum yield, which is expected to vary for different excited states. To put the relative photodissociation cross-sections on an absolute scale additional information about the photodissociation quantum yield is required.

The most straightforward way of tying the photodissociation cross-sections to an absolute frame of reference is to postulate that the excitation into the $3\nu_1$ state of HNO$_4$—the highest energy feature in the spectrum—results in 100% dissociation. The $3\nu_1$ state of HNO$_4$ lies some 2000 cm^{-1} above the known dissociation limit of the molecule. Because no barrier to dissociation is expected for a simple bond fission of this kind, a HNO$_4$ molecule excited in this transition should fragment within a few vibrational periods. With the assumption of unit photodissociation quantum yield for the $3\nu_1$ state, the absolute photodissociation band strengths $\int \sigma_{diss,\nu}\,d\nu = \int \sigma_{abs,\nu}\phi_\nu\,d\nu$ (ϕ_ν is the quantum yield) for the other overtone vibrations of HNO$_4$ can be determined relative to $3\nu_1$ as follows:

$$\int \sigma_{abs,\nu}\phi_\nu\,d\nu = \left(\frac{\int \sigma_{diss,\nu}\,d\nu}{\int \sigma_{diss,3\nu_1}\,d\nu} \times \int \sigma_{abs,3\nu_1}\,d\nu \right) \quad (6)$$

where $\int \sigma_{abs,3\nu_1}\,d\nu = 3.3 \times 10^{-20}$ cm^2 molecule^{-1} cm^{-1} (Table 1). Effective temperature-dependent quantum yields for each vibrational band are similarly determined by combining the integrated absorption cross-sections with the temperature-dependent photodissociation band strengths.

Photodissociation band strengths and quantum yields are shown in Figure 5. For the purposes of atmospheric modeling, the integrated photodissociation cross-sections and quantum yields were fitted to purely empirical functions of temperature in a manner common for kinetics measurements (summarized in Table 3). Significant extrapolation beyond the temperature and pressure range used in this study should be done with caution. It is likely, for example, that the quantum yield for $2\nu_1$ may be lower at one atmosphere total pressure.

Unfortunately, we have no convenient way of experimentally verifying the assumption of the unit photodissociation efficiency for the $3\nu_1$ state (i.e., $\phi_{3\nu_1} = 1$). One obvious approach would involve a comparison of the relative photodissociation intensities from two separate bands above the dissociation limit, say of $3\nu_1$ and $4\nu_1$, with their corresponding relative intensities in the
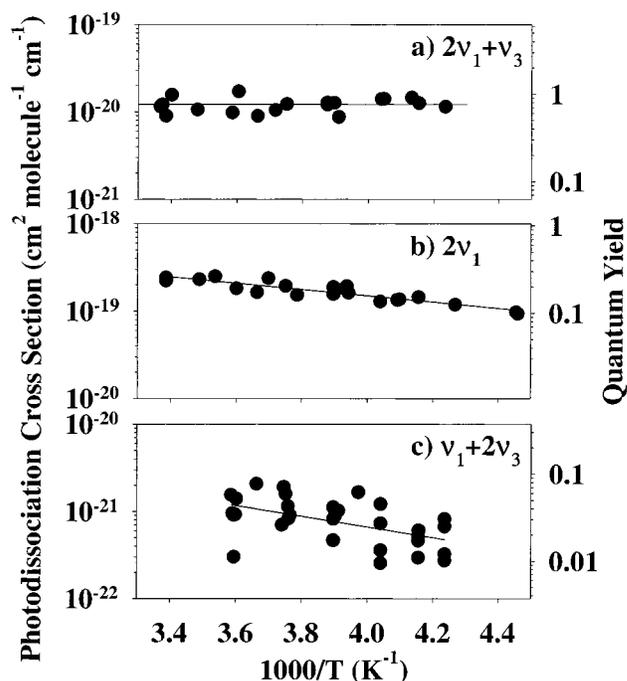
Figure 5. Plots of the photodissociation band strengths and quantum yields versus inverse temperature for (a) $2\nu_1 + \nu_3$, (b) $2\nu_1$, and (c) $\nu_1 + 2\nu_3$. The empirical fits to the data are given in Table 3.

absorption spectrum. As the $4\nu_1$ band falls outside our OPO scanning range and the band strengths for higher overtones are not known with sufficient accuracy, the only band available for such a comparison is the $2\nu_1 + \nu_3$ combination band at 8250 cm^{-1}. The position of this state with respect to the HNO$_4$ dissociation limit (7970 ± 280 cm^{-1})[5] is, however, somewhat uncertain rendering the intensity comparison less conclusive. Nevertheless, the photolysis quantum yield of 0.76 ± 0.25 with no significant temperature dependence inferred for this state is consistent with the assumption of the unity dissociation quantum yield for states above the dissociation threshold.

As the photodissociation experiments are conducted at nontrivial pressures of the buffer gas (2−40 Torr), competition between various collision-induced processes and the intramolecular energy transfer leading to dissociation of the excited HNO$_4$ molecule has to be considered. A photodissociation quantum yield of unity, as assumed here for the $3\nu_1$ state, would require dissociation to occur on a sufficiently faster time scale than the rate of vibrational quenching of the excited molecules. Rotational energy transfer normally occurs on the time scale of hard sphere collisions ($\approx 10^7$ s^{-1} at 1 Torr), whereas vibrational energy quenching usually proceeds at a much slower rate. We have conducted simple RRKM calculations that show for the internal energy of the $3\nu_1$ state, the unimolecular dissociation of HNO$_4$ occurs at a microcanonical rate of $\approx 10^{11}$ s^{-1}. Details of the RRKM calculations are not reported here, except for the fact that input parameters were chosen to provide the best fit for the pressure-dependent HNO$_4$ unimolecular decomposition rate data.[5,20] The several orders of magnitude difference between the decomposition rate and the collision rate strengthens the validity of the $\phi_{3\nu_1} = 1$ assumption under the conditions of our experiment.

One of the most intriguing findings of this study is the finite dissociation probabilities for excitations below the HNO$_4$ dissociation threshold. Bands lying below $D_0 = 7970 \pm 280$ cm^{-1} by as much 1720 cm^{-1} ($\nu_1 + 2\nu_3$) and 1070 cm^{-1} ($2\nu_1$) reproducibly appear in the photodissociation spectrum. Simple

Photodissociation of Peroxynitric Acid

J. Phys. Chem. A, Vol. 106, No. 15, 2002 **3771**

TABLE 3: Temperature-Dependent Photodissociation Cross-Sections, Dissociation Quantum Yields, and Clear Sky Atmospheric Photodissociation Rates for Several Overtone and Combination Bands of HNO$_4$[a]

band	band center (cm^{-1})	$\int \sigma_{\mathrm{diss},\nu}\phi_\nu \, d\nu$ (cm^2 molecule^{-1} cm^{-1})	quantum yield	solar flux[24] ($\times 10^{13}$ photons cm^{-2} s^{-1}/cm^{-1})	photolysis rate ($\times 10^{-6}$ s^{-1})
$4\nu_1$	13105		1	2.51	0.075
$3\nu_1$	10090		1	3.72	1.23
$2\nu_1 + \nu_3$	8240	1.21×10^{-20}	0.76	4.36	0.53
$2\nu_1$	6900	$4.09 \times 10^{-18}e^{(-826.5/T)}$ (295 K > T > 224 K)	0.14 (at 240 K)	4.90	6.41 (at 240 K)
$\nu_1 + 2\nu_3$	6250	$1.87 \times 10^{-19}e^{(-1410.7/T)}$ (278 K > T > 240 K)	0.02 (at 240 K)	5.10	0.027 (at 240 K)

J(total, 240 K) = 8.3

[a] The uncertainty in the pre-exponential factor is dominated by the uncertainty in the $3\nu_1$ band strength (20%) while the uncertainty in the exponential factor is statistical error associated with the empirical fit of the data (10% for $2\nu_1$ and 29% for $\nu_1 + 2\nu_3$). The combined clear sky photodissociation rate is on the order of 1×10^{-5} s^{-1} at 240 K, largely invariant with changes in the solar zenith angle.

back-of-the-envelope calculations, as well as direct power dependence measurements, indicate that multiphoton photodissociation processes (IR + probe or IR + IR) are not responsible. There are two mechanisms of supplying enough energy for dissociation: collision-induced activation of pre-excited molecules and coupling of internal rotational and vibrational energy into the dissociation coordinate. Although both mechanisms are likely to be important under the present experimental conditions, the lack of a pressure dependence on the integrated photodissociation band strengths suggests that a rapid intramolecular energy redistribution may be the dominant source of the near-threshold photodissociation.

In the case of the near-threshold photodissociation of NO$_2$, an excellent fit to the wavelength-dependent photodissociation quantum yield was obtained with a simple model that assumed that all molecules with total (i.e., $h\nu$ + internal) energy above D_0 fall apart.[21] Even better agreement with experimental data was obtained if a simple collision excitation treatment was included.[22] We have modeled the observed HNO$_4$ quantum yields in a similar way treating the molecule as a near-prolate symmetric top with $(B + C)/2 = 0.1345$ cm^{-1} and $A = 0.4001$ cm^{-1}. The twelve fundamental vibrations of HNO$_4$ were treated as harmonic oscillators and the internal energy probability distribution was calculated according to

$$P(E) = \frac{(2J + 1)}{Q} \times e^{-(E_{\mathrm{vibr}}(n_1, n_2, \ldots n_{12}) + E_{\mathrm{rot}}(J,K))/kT} \qquad (7)$$

using explicit counting over all possible combinations of vibrational and rotational quantum numbers with energies below 4000 cm^{-1}. In eq 7, Q is the vibration–rotation partition function, J is the overall angular momentum ($J = 0, 1, 2, \ldots$), and K, which runs from $-J$ to J, is the projection of J on the A-axis of the molecule.

The results are shown in Figure 6 for two temperatures, 273 and 223 K. The top panel shows the total vibration–rotation energy distribution. The distribution is substantially broader than one would calculate from the rotational energy levels alone because of the large number of low-frequency vibrations in HNO$_4$. In fact, the mean rotational energy of HNO$_4$, $\langle E_{\mathrm{rot}}(273\,K)\rangle \approx 285$ cm^{-1}, is lower than the mean vibrational energy, $\langle E_{\mathrm{vib}}(273\,K)\rangle \approx 380$ cm^{-1}, for the entire range of temperatures employed in the present work. The influence of the lowest frequency modes can be seen in Figure 6 as partially resolved humps on top of the internal energy distribution profile. At higher total energies, the distribution approaches a classical exponentially decaying limit.

In the lower panel of Figure 6, the probability that the internal energy will exceed a given energy threshold and the experimentally determined quantum yields for the $\nu_1 + 2\nu_3$ and $2\nu_1$
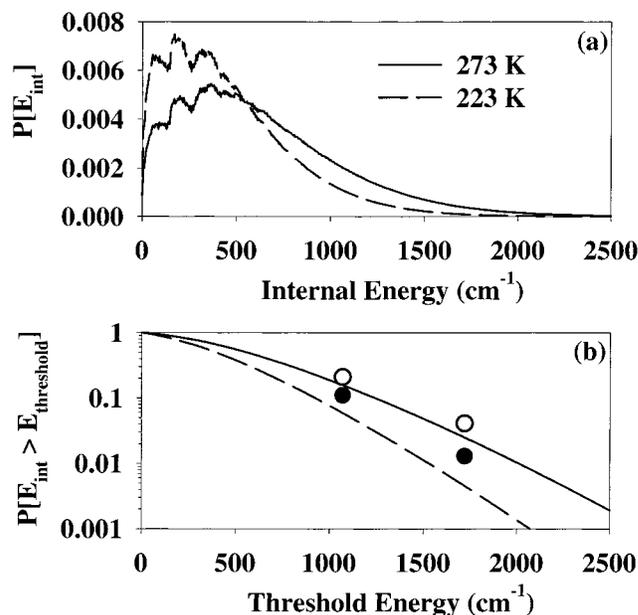
Figure 6. Calculated HNO$_4$ vibration–rotation energy distribution. (a). Internal energy distribution of HNO$_4$ at 273 K (solid line) and 223 K (dashed line). (b). Probability that the internal energy of HNO$_4$ exceeds a given energy threshold (lines). Experimentally measured quantum yields for $2\nu_1$ and $\nu_1 + 2\nu_3$ bands, which lie 1070 and 1720 cm^{-1} below D_0, respectively, are shown as open (273 K) and closed (223 K) circles. Adjusting the dissociation energy of HNO$_4$ by a mere 200 cm^{-1} would greatly improve the agreement between the model and experiment.

bands are shown. Satisfactory agreement between these two values is observed using this simplistic Boltzmann model treatment. Better agreement is obtained if the dissociation energy of HNO$_4$ is reduced by just 200 cm^{-1}, well within the error bars of the presently accepted value ($D_0 = 7970 \pm 280$ cm^{-1}).[5] The neglect of collision effects and the relatively large uncertainty associated with the reported quantum yields do not, however, justify the adjustment to D_0 based on the results presented here; a spectroscopically accurate determination of HNO$_4$ dissociation energy would greatly aid in the interpretation of the photodissociation yields.

C. Atmospheric Implications. Observation of large near-IR photodissociation probabilities of HNO$_4$, especially for the $2\nu_1$ band, confirms the importance of overtone driven photochemistry in the atmosphere and supports the suggestion that HNO$_4$ is the missing source for HO$_x$ production in the lower stratosphere at high solar zenith angles. The clear sky near-IR photolysis rate for HNO$_4$, J(HNO$_4$), can be estimated for each vibrational band using the relationship:

$$J(\mathrm{HNO_4}) = \int \sigma_{\mathrm{diss}}(\nu,T)I(\nu)\,\mathrm{d}\nu \cong \langle I(\nu)\rangle \int \sigma_{\mathrm{diss}}(\nu,T)\,\mathrm{d}\nu \quad (8)$$

where $\sigma_{\mathrm{diss}}(\nu,T)$ is the temperature- and frequency-dependent photodissociation cross-section of $\mathrm{HNO_4}$ as measured in the action spectra and $I(\nu)$ is the frequency-dependent top of the atmosphere solar radiance. Negligible scattering or absorption is expected at these wavelengths (the $\mathrm{H_2O}$ overtones are sufficiently shifted to the blue and do not provide significant attenuation in the stratosphere and upper troposphere). For these calculations, the reflectivity of the surface (albedo) is assumed to be 0. Results for the individual bands and for the sum of all known bands at a temperature of 240 K are given in Table 3. The total photolysis rate of 8.3×10^{-6} s^{-1} obtained here is in good agreement with that required to match the missing HO$_x$ source (J-value = 1×10^{-5} s^{-1}) as depicted in Figure 1 of Wennberg et al.[10] Incorporation of these near-IR photolysis rates into a photochemical model was also found to significantly improve the simulations of solar occultation Fourier Transform spectroscopy (FTS) measurements of $\mathrm{HNO_4}$ obtained in the stratosphere.[23] Particularly at high latitudes, where the sun never reaches high into the sky, the near-IR photolysis of $\mathrm{HNO_4}$ contributes significantly to the total loss rate of this important reservoir. Calculations that neglect this process overestimate the rate of reaction 3 and therefore underestimate the average OH density.

Supporting Information Available: Table of the peroxynitric acid photodissociation band strengths and photodissociation rate versus inverse temperature. This material is available free of charge via the Internet at http://pubs.acs.org.

References and Notes

(1) Donaldson, D. J.; Frost, G. J.; Rosenlof, K. H.; Tuck, A. F.; Vaida, V. *Geophys. Res. Lett.* **1997**, *24*, 2651.

(2) Crim, F. F. *Annu. Rev. Phys. Chem.* **1984**, *35*, 657.

(3) Phillips, J. A.; Orlando, J. J.; Tyndall, G. S.; Vaida, V. *Chem. Phys. Lett.* **1998**, *296*, 377.

(4) Lange, K. R.; Wells, N. P.; Plegge, K. S.; Phillips, J. A. *J. Phys. Chem. A* **2001**, *105*, 3481.

(5) Zabel, F. *Z. Phys. Chem.* **1995**, *188*, 119.

(6) Rinsland, C. P.; Zander, R.; Farmer, C. B.; Norton, R. H.; Brown, L. R.; Russell, J. M., III; Park, J. H. *Geophys. Res. Lett.* **1986**, *13*, 761.

(7) Brasseur, G.; Solomon, S. *Aeronomy of the middle atmosphere: chemistry and physics of the stratosphere and mesosphere*; D. Reidel Pub. Co.: Hingham, MA, 1984. Sold and distributed in the United States and Canada by Kluwer Academic Publishers.

(8) Jaegle, L.; Jacob, D. J.; Brune, W. H.; Wennberg, P. O. *Atmos. Environ.* **2001**, *35*, 469.

(9) Folkins, I.; Wennberg, P. O.; Hanisco, T. F.; Anderson, J. G.; Salawitch, R. J. *Geophys. Res. Lett.* **1997**, *24*, 3185.

(10) Wennberg, P. O.; Salawitch, R. J.; Donaldson, D. J.; Hanisco, T. F.; Lanzendorf, E. J.; Perkins, K. K.; Lloyd, S. A.; Vaida, V.; Gao, R. S.; Hintsa, E. J.; Cohen, R. C.; Swartz, W. H.; Kusterer, T. L.; Anderson, D. E. *Geophys. Res. Lett.* **1999**, *26*, 1373.

(11) Zhang, H.; Roehl, C. M.; Sander, S. P.; Wennberg, P. O. *J. Geophys. Res.* **2000**, *105*, 14593.

(12) Kenley, R. A.; Trevor, P. L.; Lan, B. Y. *J. Am. Chem. Soc.* **1981**, *103*, 2206.

(13) Appelman, E. H.; Gosztola, D. J. *Inorg. Chem.* **1995**, *34*, 787.

(14) Wu, S.; Blake, G. A.; Sun, Z. Y.; Ling, J. W. *Appl. Opt.* **1997**, *36*, 5898.

(15) Wennberg, P. O.; Cohen, R. C.; Hazen, N. L.; Lapson, L. B.; Allen, N. T.; Hanisco, T. F.; Oliver, J. F.; Lanham, N. W.; Demusz, J. N.; Anderson, D. E. *Rev. Sci. Instrum.* **1994**, *65*, 1858.

(16) May, R. D.; Friedl, R. R. *J. Quant. Spectrosc. Radiat. Transfer* **1993**, *50*, 257.

(17) Niki, H.; Maker, P. D.; Savage, C. M.; Breitenbach, L. P. *Chem. Phys. Lett.* **1977**, *45*, 564.

(18) Friedl, R. R.; May, R. D.; Duxbury, G. *J. Mol. Spectrosc.* **1994**, *165*, 481.

(19) Chen, Z.; Hamilton, T. P. *J. Phys. Chem.* **1996**, *100*, 15731.

(20) Graham, R. A.; Winer, A. M.; Pitts, J. N., Jr. *J. Chem. Phys.* **1978**, *68*, 4505.

(21) Pitts, J. N., Jr.; Sharp, J. H.; Chan, S. I. *J. Chem. Phys.* **1964**, *40*, 3655.

(22) Roehl, C. M.; Orlando, J. J.; Tyndall, G. S.; Shetter, R. E.; Vázquez, G. J.; Cantrell, C. A.; Calvert J. G. *J. Phys. Chem.* **1994**, *98*, 7837.

(23) Salawitch, R. J., et al. Manuscript in preparation.

(24) *Allen's Astrophysical Quantities*, 4th ed.; Allen, C. W., Ed.; Springer-Verlag: New York, 2000; Section 14.6.